Analysis of Self-Oscillating DC-DC Resonant Power Converters using a Hysteretic Relay

David R. Williams, C. Bingham, D.A. Stone, M.P. Foster, A. Gilbert
Sheffield University
Mappin Building, Mappin Street
Sheffield, England
Phone: +44 (0) 114-2225847
Email: elp05drw@sheffield.ac.uk

Keywords

<<Resonant converter>>, <<DC power supply>>, <<ZVS converters>>.

Abstract

The paper presents a technique for exciting resonant DC-DC converters in a self-oscillating manner. The analysis necessary to predict the behaviour of such converters is also given. The oscillation is based on the behaviour of a hysteretic relay with a negative hysteresis transition. Self-oscillating converters benefit from higher efficiency/higher power density than their non-self-oscillating counterparts as they can be operated closer to the tank resonant frequency. The self-oscillating mechanism presented here is also simple and cost effective to implement. A prototype converter is presented in order to verify the theoretical claims.

Introduction

In recent times, there has been a growing interest in driving resonant converters in a self-oscillating manner. Whilst such techniques have become common-place in lamp-ballasts[1], self-oscillating control techniques are only just beginning to gain sway in the field of DC-DC resonant converters, principally because of the added complication involved in designing the converter and control system.

There are a number of advantages to allowing a converter to self oscillate compared to forced frequency control techniques, which have traditionally been more popular with DC-DC converters. The most prominent advantage is that it compensates for variations in the tolerances of components, allowing the converter to be driven much closer to resonance whilst maintaining zero-voltage switching (ZVS). This compares very favourably with forced-frequency control techniques, where the designer must allow some tolerance between the lowest frequency at which the converter will operate, and the converter's real resonant frequency (see Figure 1).

In the field of DC-DC converter technology, self-oscillating converters are scarce, with externally imposed switching frequencies being used in the majority of cases. There are a number of approaches to inducing self-oscillation in a resonant converter. One example is phase or power-factor control. Such schemes work by timing the length of a converter cycle, and using the information to calculate the time at which the inverter stage of the converter should switch to apply a particular phase difference between the converter input current and voltage, thereby controlling the power factor, and the amount of real power is transfered [2]. Another approach is to sense some aspect of the resonant tank, and switch when the signal passes through certain points [3]. There a number of ways of modelling this behaviour, relay systems being a prime candidate [4, 1, 5].

Here then, an analysis technique is described for low-cost self-oscillating LCLC resonant DC-DC converters using relay systems theory in order to predict steady-state oscillation behaviour using non-computationally intensive methods[1]. The converter chosen is a series-parallel LCLC topology (see Figure 2). This topology has the advantage that parasitics in an isolating transformer can readily be incorporated into the design of the resonant tank (L_p and L_s being mainly attributed to a transformer's $L_{magnetisation}$ and L_{stray} respectively). However, it should be noted that the underlying principles are ultimately applicable to the wider field of resonant converter topologies.

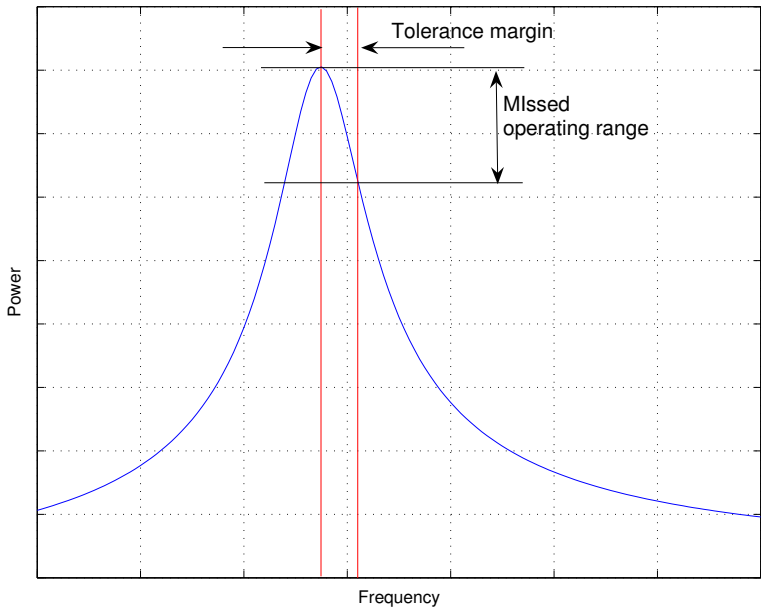

Figure 1: Unused capability in a conventional resonant DC-DC converter

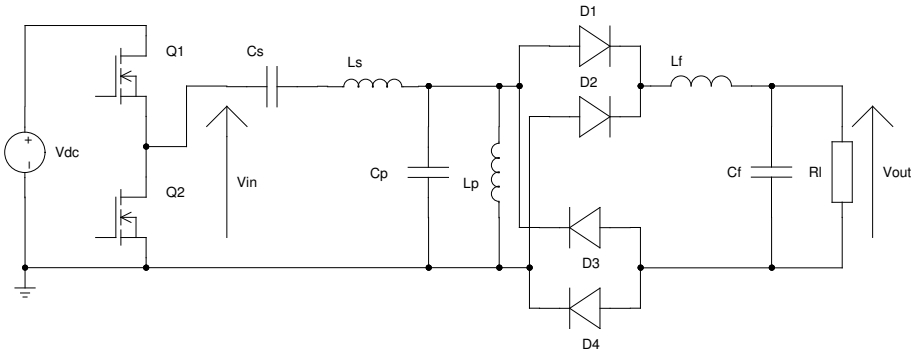

Figure 2: Circuit diagram of power section of self oscillating converter

Relay System Analysis

For the converter to self-oscillate, the switching instances are dictated by the current through the series inductor (i_{L_s}). Switching occurs when i_{L_s} passes through certain values, as shown in Figure 3. This in effect allows the frequency of the converter to be controlled by changing the value of i_{L_s} at which the switching instance occurs. Altering the value of i_{L_s} at which the input voltage is switched has the effect of altering the phase difference (P) between the driving voltage V_{in} and the inductor current, thereby altering the power-factor of the converter and allowing the amount of real power delivered into the converter to be controlled. Thus, a mechanism exists for controlling the proximity to the resonant frequency at which the converter operates, but without dictating the frequency in the control system. The lower the value of i_{L_s} at which the driving voltage is switched, the closer the converter operates to the resonant frequency. Exciting the converter with the hysteresis width (ε) set to 0 puts V_{in} and i_{L_s} in phase, and the converter runs at its resonant frequency. To achieve the desired effect, a hysteretic relay with a negative hysteresis band (characteristic shown in Figure 4(a)) is used to control the switches [1, 4].

To analyse the system using relay systems techniques, a linear approximation of the converter and load must first be made. For this purpose, a fundamental mode approximation (FMA) [6, 7] is used to replace the load and rectifier with a simple resistor. Using this approximation, the conductance of the circuit as

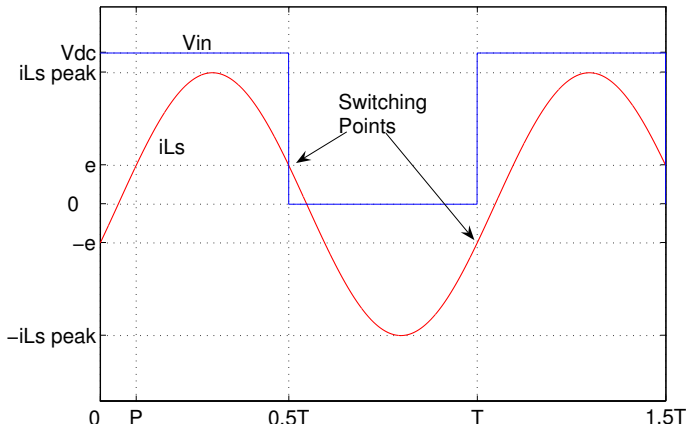

Figure 3: Switching instance in a self-oscillating resonant converter

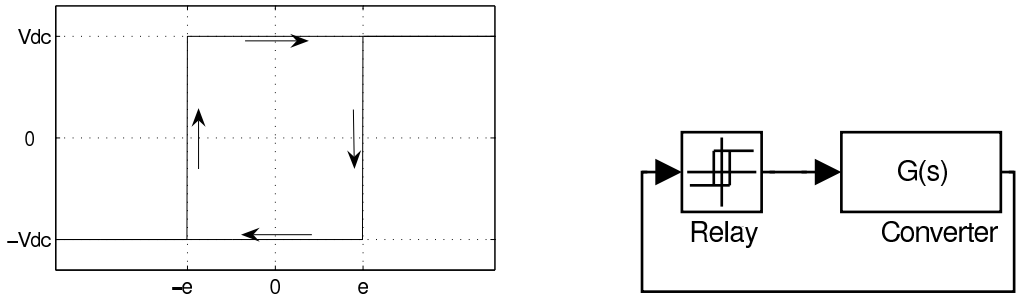

(a) Hysteresis characteristic of relay

(b) Closed loop of converter

Figure 4: Relay and system

seen by the power switches can be calculated easily using simple linear circuit analysis.

$$
\begin{aligned}
Y_{tank} = \frac{
&-(C_pC_sL_pR_{l_{FMA}} + C_pC_sL_pR_{C_p})j\omega^3 \\
&-((C_pC_sR_{l_{FMA}} + C_pC_sR_{C_p})R_{L_p} + C_pC_sR_{C_p}R_{l_{FMA}} + C_sL_p)\omega^2 \\
&+(C_sR_{L_p} + C_sR_{l_{FMA}})j\omega \\
&\hline
&C_pC_sL_pL_s(R_{l_{FMA}} + R_{C_p})\omega^4 \\
&-(C_pC_sL_p(R_{l_{FMA}}(R_{L_s} + R_{C_s} + R_{C_p}) + R_{C_p}(R_{L_s} + R_{C_s})) \\
&+C_pC_sL_s(R_{l_{FMA}}(R_{C_p} + R_{L_p}) + R_{C_p}R_{L_p}) + C_sL_pL_s)j\omega^3 \\
&-(C_pC_s(R_{l_{FMA}}(R_{L_p}(R_{L_s} + R_{C_s} + R_{C_p}) + R_{C_p}(R_{L_s} \\
&+R_{C_s})) + R_{C_p}R_{L_p}(R_{L_s} + R_{C_s})) \\
&+C_sL_p(R_{L_s} + R_{l_{FMA}} + R_{C_s}) + C_sL_s(R_{L_p} + R_{l_{FMA}}) \\
&+C_pL_p(R_{lFMA} + R_{C_p}))\omega^2 \\
&+(C_s(R_{l_{FMA}}(R_{L_s} + R_{L_p} + R_{C_s}) + R_{L_p}(R_{L_s} + R_{C_s})) \\
&+C_p(R_{l_{FMA}}(R_{L_p} + R_{C_p}) + R_{C_p}R_{L_p}) + L_p)j\omega \\
&+R_{l_{FMA}} + R_{L_p}
\end{aligned}
\tag{1}
$$

s can be substituted for $j\omega$ to become the transfer function from V_{in} to i_{L_s}:

$$G_{tank}(s) = \frac{\begin{array}{r}(C_pC_sL_pR_{l_{FMA}} + C_pC_sL_pR_{C_p})s^3 \\ +((C_pC_sR_{l_{FMA}} + C_pC_sR_{C_p})R_{L_p} + C_pC_sR_{C_p}R_{l_{FMA}} + C_sL_p)s^2 \\ +(C_sR_{L_p} + C_sR_{l_{FMA}})s\end{array}}{\begin{array}{r}C_pC_sL_pL_s(R_{l_{FMA}} + R_{C_p})s^4 \\ +(C_pC_sL_p(R_{l_{FMA}}(R_{L_s} + R_{C_s} + R_{C_p}) + R_{C_p}(R_{L_s} + R_{C_s})) \\ +C_pC_sL_s(R_{l_{FMA}}(R_{C_p} + R_{L_p}) + R_{C_p}R_{L_p}) + C_sL_pL_s)s^3 \\ +(C_pC_s(R_{l_{FMA}}(R_{L_p}(R_{L_s} + R_{C_s} + R_{C_p}) + R_{C_p}(R_{L_s} \\ +R_{C_s})) + R_{C_p}R_{L_p}(R_{L_s} + R_{C_s})) \\ +C_sL_p(R_{L_s} + R_{l_{FMA}} + R_{C_s}) + C_sL_s(R_{L_p} + R_{l_{FMA}}) \\ +C_pL_p(R_{lFMA} + R_{C_p}))s^2 \\ +(C_s(R_{l_{FMA}}(R_{L_s} + R_{L_p} + R_{C_s}) + R_{L_p}(R_{L_s} + R_{C_s})) \\ +C_p(R_{l_{FMA}}(R_{L_p} + R_{C_p}) + R_{C_p}R_{L_p}) + L_p)s \\ +R_{l_{FMA}} + R_{L_p}\end{array}} \tag{2}$$

The transfer function can then be used in closed-loop with the hysteretic relay to model the self-oscillating converter, as in Figure 4(b). To begin the analysis, the switching instants are first defined mathematically. From Figure 3, it can be seen that at switching instants, the following are true:

$$\left.\begin{array}{r} i_{L_s} = \varepsilon \\ \dfrac{di_{L_s}}{dt} < 0 \end{array}\right\} \text{When } V_{in} \text{ switches negative} \tag{3}$$

$$\left.\begin{array}{r} i_{L_s} = -\varepsilon \\ \dfrac{di_{L_s}}{dt} > 0 \end{array}\right\} \text{When } V_{in} \text{ switches positive} \tag{4}$$

The voltage supplied to the convert (V_{in}) can be modelled as the sum of a series of alternating step inputs, giving an effective square wave. In steady state, the series can be extended backwards in time ad infinitum:

$$V_{in} = V_{dc}\left\{\sum_{k=0}^{\infty}\left[H\left(t+kT\right) - H\left(t-\frac{T}{2}+kT\right)\right]\right\} \tag{5}$$

where $H(t)$ is the Heaviside step function. For the period $0 \leq t < T/2$, (5) can be manipulated to (6):

$$V_{in} = V_{dc}\left\{H(t) + \sum_{k=1}^{\infty}\left[H\left(t+kT\right) - H\left(t-\frac{T}{2}+kT\right)\right]\right\} \tag{6}$$

The transfer function of the resonant tank from (2) can be broken down into its constituent poles, as follows:

$$G_{tank}(s) = \frac{P(s)}{Q(s)} = \sum_{k=1}^{n}\frac{A_k}{s-p_k} \tag{7}$$

$$A_k = \frac{P(p_k)}{Q'(p_k)} \tag{8}$$

$$Q'(s) = \frac{dQ(s)}{ds} \tag{9}$$

where p_k is a pole of $G(s)$, and n is the number of poles of $G(s)$. The transient step response can be found by taking the inverse Laplace transform of (7) with a step applied as follows:

$$q(t) = \mathcal{L}^{-1}\left(\frac{G(s)}{s}\right) = A_0 + \sum_{k=1}^{n}\frac{A_k}{p_k}e^{p_kt} \tag{10}$$

Convolving the step response with the series of voltage steps that constitute V_{in} for the first half-period ($0 \leq t < T/2$), the steady state waveform of $i_{L_s}(t)$ can be described by:

$$i_{L_s}(t) = V_{dc}\left\{ q(t) + \sum_{m=1}^{\infty}\left[q\left(t+mT\right) - q\left(t-\frac{T}{2}+mT\right)\right]\right\} \tag{11}$$

$$\begin{aligned} &= V_{dc}\left\{ A_0 + \sum_{k=1}^{n}\frac{A_k}{p_k}e^{p_k t}\right. \\ &\quad \left. + \sum_{m=1}^{\infty}\left[\sum_{k=1}^{n}\frac{A_k}{p_k}e^{p_k(t+mT)} - \sum_{k=1}^{n}\frac{A_k}{p_k}e^{p_k\left(t-\frac{T}{2}+mT\right)}\right]\right\} \end{aligned} \tag{12}$$

$$= V_{dc}\left\{ q(t) + \sum_{k=1}^{n}\left[\frac{A_k}{p_k}e^{p_k t}\left(1-e^{\frac{-p_k T}{2}}\right)\sum_{m=1}^{\infty}e^{p_k mT}\right]\right\} \tag{13}$$

$$= V_{dc}\left\{ q(t) + \sum_{k=1}^{n}\frac{A_k}{p_k}e^{p_k t}\left(\frac{e^{p_k T}-e^{\frac{p_k T}{2}}}{1-e^{p_k T}}\right)\right\} \tag{14}$$

For the period 0 to $T/2$ (Figure 3), (14) applies. As the period from $T/2$ to T is just an inverted form of the waveform in the first half period, the equations that describe it are similar:

$$i_{L_s}(t) = V_{dc}\left\{ -q\left(t-\frac{T}{2}\right) - \sum_{k=1}^{n}\frac{A_k}{p_k}e^{p_k\left(t-\frac{T}{2}\right)}\left(\frac{e^{p_k T}-e^{\frac{p_k T}{2}}}{1-e^{p_k T}}\right)\right\} \tag{15}$$

Equivalently, the derivative of i_{L_s} is given by:

$$\frac{di_{L_s}(t)}{dt} = \begin{cases} V_{dc}\left[l(t) + \sum_{k=1}^{n} A_k e^{p_k t}\left(\frac{e^{p_k T}-e^{\frac{p_k T}{2}}}{1-e^{p_k T}}\right)\right] & \text{when } 0 < t \leq \frac{T}{2} \\ V_{dc}\left[-l\left(t-\frac{T}{2}\right) - \sum_{k=1}^{n} A_k e^{p_k\left(t-\frac{T}{2}\right)}\left(\frac{e^{p_k T}-e^{\frac{p_k T}{2}}}{1-e^{p_k T}}\right)\right] & \text{when } \frac{T}{2} < t \leq T \end{cases} \tag{16}$$

where

$$l(t) = \mathcal{L}^{-1}\{G_{tank}(s)\} = \sum_{k=1}^{n} A_k e^{p_k t} \tag{17}$$

Using the results in (14), (15) and (16), it is apparent that:

$$i_{L_s}\left(\frac{T}{2}\right) = V_{dc}\left\{ -\sum_{k=1}^{n}\frac{A_k}{p_k}\left(\frac{e^{p_k T}-e^{\frac{p_k T}{2}}}{1-e^{p_k T}}\right)\right\} \tag{18}$$

$$\frac{di_{L_s}\left(\frac{T}{2}\right)}{dt} = V_{dc}\left\{ -\sum_{k=1}^{n} A_k\left(\frac{e^{p_k T}-e^{\frac{p_k T}{2}}}{1-e^{p_k T}}\right)\right\} \tag{19}$$

Since T represents the period of oscillation, $\frac{1}{f}$ may be substituted in its place in (18) and (19):

$$H(f) = i_{L_s}\left(\frac{1}{2f}\right) = V_{dc}\left\{ -\sum_{k=1}^{n}\frac{A_k}{p_k}\left(\frac{e^{\frac{p_k}{f}}-e^{\frac{p_k}{2f}}}{1-e^{\frac{p_k}{f}}}\right)\right\} \tag{20}$$

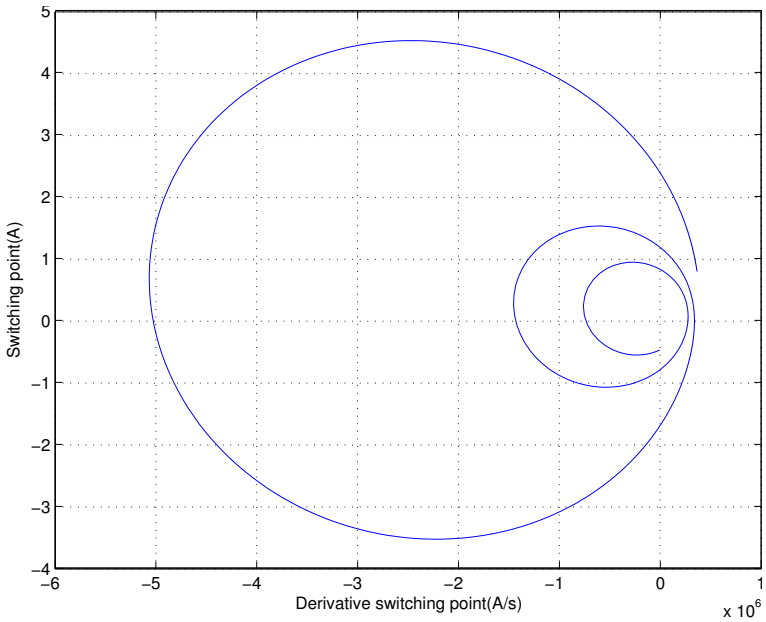

Figure 5: Hamel locus for a 4th order converter

Parameter	Value
L_s	$11.2\mu H$
R_{L_s}	$115m\Omega$ (incorporates $R_{DS_{on}}$)
C_s	$0.4\mu F$
R_{C_s}	$20m\Omega$
L_p (transformer)	$107.8\mu H$
R_{L_p}	$20m\Omega$
C_p	$0.4\mu F$
R_{C_p}	$20m\Omega$
R_l	22Ω

Table I: Resonant converter parameters

$$H'(f) = \frac{di_{L_s}\left(\frac{1}{2f}\right)}{dt} = V_{dc}\left\{-\sum_{k=1}^{n} A_k\left(\frac{e^{\frac{p_k}{f}} - e^{\frac{p_k}{2f}}}{1-e^{\frac{p_k}{f}}}\right)\right\} \tag{21}$$

Equations (20) and (21) can now be used to plot the Hamel locus for the linearised resonant converter. The resultant plot is shown in Figure 5. Using the Hamel locus it is possible to identify possible modes of oscillation for a given value of hysteresis width (ε) used in the relay controlling the switches. The Hamel locus is used because the dominant oscillatory mode always forms the outer-most loop, and so the mode that a real oscillating converter will adopt may be readily identified.

Practical Converter

To verify the analysis in the preceding sections, a prototype converter is realised. For the purposes of demonstrating a working self-oscillating fourth order DC-DC supply, a converter is specified to convert ∼25W from 9V up to 18V. The resonant peak at 107.8kHz is the designed operating resonance.

The control system is implemented on a Xilinx CPLD and a Microchip PIC microcontroller, along with some analogue sensing-electronics.

The series inductor current is not measured directly for the controller, but inferred from measurements of the voltage across the series inductor, as this is likely to be the technique envisaged in a commercial solution, since current sensing is prohibitively expensive. It is notable that certain regions in the Hamel locus are not single-valued functions of the switching threshold set on the series inductor current. In practice this is overcome by switching at certain points on the differential waveform (v_{L_s}) in those regions.

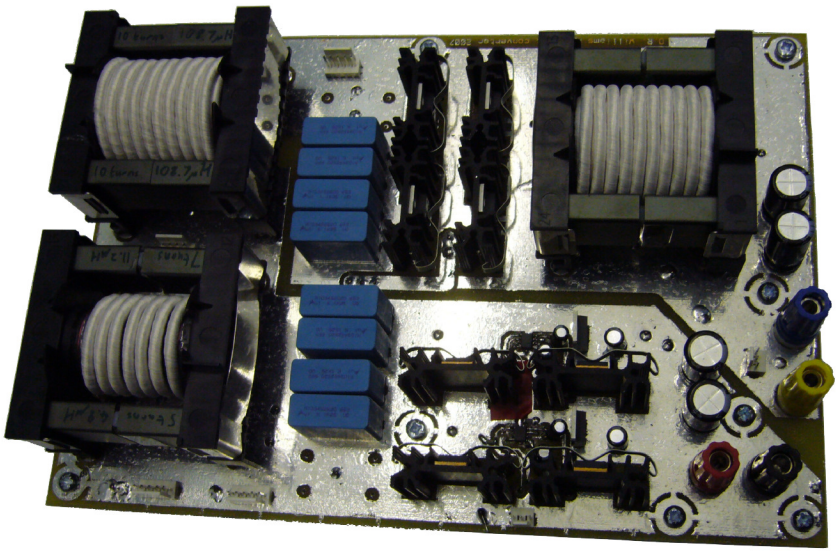

Figure 6: Converter used to demonstrate self-oscillating control

Comparing the results with those from the analysis and simulations in Simulink®, and plotting the relevant Hamel loci yields a reasonable correlation (Figure 7).

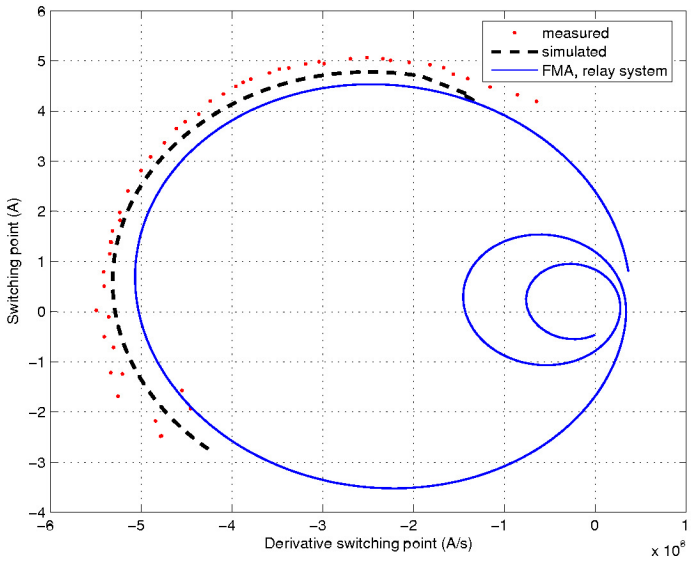

Figure 7: Hamel locus of calculated, real and simulated converter

Modification to FMA approximation

The main reason for the apparent disparity between the Hamel locus of the simulated and real converters and that of the relay systems analysis (shown together in Figure 7) relates to the use of the FMA approximation. The main problem is FMA's over-simplification of a full-wave rectifier with a smoothing inductor. An improved model can be obtained by accounting for the diode on-state voltages as follows.

An approximation of the rectifier input voltage waveform is obtained using standard FMA analysis (where $R_{l_{FMA}} = \frac{\pi^2}{8} R_l$). The absolute value of this waveform is then averaged over one period:

$$\begin{aligned} V_{absav} &= \int_0^T \left| v_{C_p}(t) \right| dt \\ &= \frac{2}{\pi} \hat{v}_{C_p} \end{aligned} \tag{22}$$

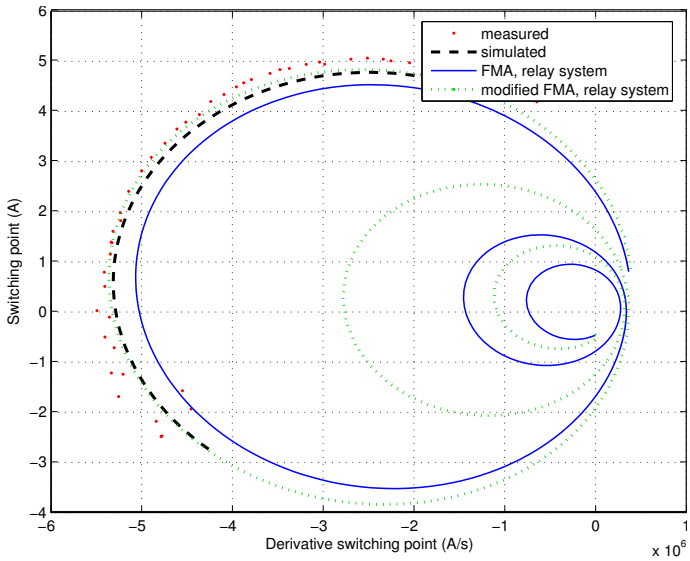

Figure 8: Hamel locus with alternative FMA approximation

Assuming the smoothing inductor forces the rectifier to conduct continuously, the average input voltage, and hence the output voltage is:

$$V_{out} = V_{absav} - V_d \tag{23}$$

The output current can then be obtained and referred back to the tank, as in standard FMA analysis

$$I_{out} = \frac{V_{out}}{R_l} \tag{24}$$

$$i_{Rect} \approx \frac{4}{\pi} I_{out} \sin(\omega t) \tag{25}$$

The rectifier, output filter and load, can thus be represented by a new 'equivalent' value of resistance:

$$R_{l_{FMAmod}} = \frac{v_{C_p}}{i_{Rect}} = \frac{\pi^2 \hat{v}_{C_p} R_l}{8\hat{v}_{C_p} - 8\pi V_d} \tag{26}$$

This set of equations can then be used in an iterative manner to provide an improved linear approximation for the load presented to the resonant tank. The result of this approximation, as applied to the relay systems analysis, is shown in the Hamel locus in Figure 8. It can be seen that the Hamel locus from this technique shows much better agreement with both the experimental and simulated results.

Conclusions

A technique for driving Resonant DC-DC converters in a self-oscillating manner has been presented. The technique offers a simple, non-computationally intensive generalised method for analysing self-oscillating resonant converters. The proposed methodology is demonstrated to work well in practice, with the predicted converter behaviour being in good agreement with that of both simulated and prototype converters. Agreement between the theory and practice can be further improved with the application of the modified FMA approximation, as outlined in the last section.

References

[1] C. Chang and G. W. Bruning, "Self-oscillating electronic ballast analysis using the relay-systems approach," *IEEE Transactions on Industry Applications*, vol. 37, pp. 255–261, January 2001.

[2] H. Pinheiro, P. K. Jain, and G. Joós, "Self-sustained oscillating resonant converters operating above the resonant frequency," *IEEE Transactions on Power Electronics*, vol. 14, pp. 803–815, September 1999.

[3] A. Forsyth and Y. Ho, "High performance control of the series-parallel resonant converter," *IEE Proceedings on Power Applications*, vol. 144, pp. 131–139, March 1997.

[4] S. Varigonda and T. T. Georgiou, "Dynamics of relay relaxation oscillators," *IEEE Transactions on Automatic Control*, vol. 46, pp. 65–77, January 2001.

[5] A. Y. Pogromsky, W. Heemels, and H. Nijmeijer, "On solution concepts and well-posedness of linear relay systems," *Automatica*, vol. 39, pp. 2139–2147, 2003.

[6] R. L. Steigerwald, "A comparison of half-bridge resonant converter topologies," *IEEE Transactions on Power Electronics*, vol. 3, pp. 174–182, April 1988.

[7] A. J. Forsyth, G. A. Ward, and S. V. Mollov, "Extended fundamental frequency analysis of the lcc resonant converter," *IEEE Transactions on Power Electronics*, vol. 18, pp. 1286–1292, November 2003.